Jacutingaite family: An efficient platform for coexistence of spin valley Hall effects, valley spin-valve realization, and layer spin crossover

Majeed Ur Rehman, Maryam Kiani, and Jian Wang [*]

College of Physics and Optoelectronic Engineering, Shenzhen University, Shenzhen, Guangdong 518060, China

Jacutingaite family, a family of naturally occurring exfoliable minerals (Pt_2HgSe_3 and Pd_2HgSe_3) discovered in Brazil, is recently predicted to be the very first large-gap Kane-Mele quantum spin Hall insulators. However, yet to date, the door is locked for realizing versatile spin-valley based phenomena due to inversion symmetry in this family. By exploiting the inversion symmetry using different strategies such as placing the jacutingaite family in the vertical electric field or growing its composites with some suitable well-matched systems, we reveal several promising valley spin based phenomena in the jacutingaite family. Overall, we achieve the coupled spin valley Hall effect, valley spin-valve effect, Rashba spin splitting around the low-symmetric M point, layer crossover accompanied by spin crossover, and selective-excitation of carriers from opposite valleys in this family. More interestingly, swapping of the induced spin splittings, Berry curvatures, and the spin texture between the two valleys occur upon the reversal of electric field from $E_z > 0$ to $E_z < 0$ without destroying the $\mathcal{Z}_2$ topological hallmarks. Meanwhile, considerable hexagonal trigonal warping effects around the K_+ and K_- valleys are realized. Furthermore, by applying vertical electric field through interfacial coupling with ferroelectric $III_2 - VI_3$ film, valley contrasting Berry curvature in the Pt_2HgSe_3 layer with a larger spin splitting in the lower conduction band (~ 188 meV) is achieved in the $+P$ polarization state. By inverting the polarization state from $+P$ to $-P$, the Fermi level shifts down into the valence band of the Pt_2HgSe_3 layer (~ 82 meV) revealing a hole doping in the Pt_2HgSe_3 layer. This could establish an effective mechanism to control doping levels in the Pt_2HgSe_3 layer as desirable for achieving superconductivity at finite doping in the jacutingaite family. Our paper provides a path towards integrating valleytronics and spintronics in multivalley materials with broken inversion symmetry.

I. INTRODUCTION

Recently, two-dimensional solids crystallized in the hexagonal lattice geometry, especially after the experimental isolation of graphene in 2004 [1] and its-like structures such as germanene and stanene etc. (also referred to as two-dimensional Xenes), have drawn great attention due to offering a versatile platform for the manipulation of charge, spin, and valley degrees freedom in the topological spintronic and valleytronics context [2–8]. The Xene solids follow the famous Kane-Mele topological model [2,9]. However, the weak spin-orbit coupling effects in graphene ($\lambda_{SO} \sim 40\ \mu$eV) and other Xene materials limit their practical applications. By further efforts, the researcher discovered a new family of the so-called transition metal dichalcogenides with strong spin-orbit coupling, offering a comparatively better platform for manipulating spin and valley-dependent properties as highly demandable for spintronic and valleytronics applications [10–13].

The recent discovery of the jacutingaite family (Pt_2HgSe_3 and Pd_2HgSe_3) is considered as an alternative of Xene family in the topological and valleytronics context. It is because jacutingaite family follows the same topological model (Kane-Mele) as Xene solids do [14]. However, this family host strong spin-orbit coupling effects ($\lambda_{SO} \sim 21$ meV) as compared to graphene and is very suitable for spin and valley related practical applications [15–17]. Very recently, it has been shown that $(Pt/Pd)_2HgSe_3$ is $\mathcal{Z}_2$ topological insulator with large nontrivial band gap ~ 0.5 eV [14]. So far, two members of this family, Pt_2HgSe_3 and Pd_2HgSe_3 have been experimentally synthesized in the bulk form [18]. Very recently, this family has been studied in the free-standing form with inversion symmetry as well as on magnetic substrate for the phenomena like quantum spin Hall (QSH) and valley-polarized quantum anomalous Hall effects respectively [15,19–22].

However, yet to date, the door is closed for various valley spin based phenomena due to the presence of inversion symmetry in the jacutingaite family. In this context, a detailed exploration on the consequences of the broken inversion symmetry in the jacutingaite family is clearly needed. This type of study is important because it may unlock the door for phenomena based on spin-valley locking and valley contrasting Berry curvature in the $(Pt/Pd)_2HgSe_3$ layers. In particular, it can reveal several interesting phenomena such as coexistence of quantum spin and quantum valley Hall (QVH) effects (i.e., quantum spin-valley Hall effect), valley-spin locking such as valley spin-valve effects, Rashba and valley Zeeman-type spin splitting in the jacutingaite family.

[*]Correspondence author: jianwang@hku.hk

While individually, many QSH insulators protected by time-reversal symmetry and QVH insulators protected by valley symmetry are available in the literature. However, so far, two-dimensional materials displaying both QVH and QSH phases at the same time are rare, and it is challenging to build a platform where both of these anomalies exist simultaneously in a single natural material. For instance, in this context, strategies such as making lateral heterostructure of two systems having QVH and QSH signatures, respectively, have been employed to realize the quantum spin-valley Hall kink states at the interface [23,24]. However, this strategy needs a sharp, well-matched, and smooth interface, making its experimental realization challenging. Thus, establishing a robust platform where both QVH and QSH features emerge simultaneously in single materials indeed would be exciting and it is one of the aims of the present study. This is because, their emergence can be used to explore the so-called coupled spin-valley Hall effects protected not only by the valley-inversion symmetry but also by the time-reversal symmetry against the nonmagnetic disorder, allowing robust ballistic spin-valley-momentum locking transport.

On other hand, examples of two-dimensional solids having features of spin-valley locking with electrically switchable nature are also rare or less explored. These effects are considered very useful for a phenomenon like the valley spin-valve effect as highly demandable for valleytronics based applications. So far, in this context, only the germanene, stanene, single-layer (bilayer) transition metal dichalcogenides in $1T'$ ($2H$) phase have been reported [25]. By exposing jacutingaite family to a vertical electric field and therefore breaking the inversion symmetry can establish a platform where the valley and spin degrees of freedom can be coupled, enabling the formation of the valley spin-valve effect. In previous reports, the robust spin-valley coupling has been confirmed to intensify the spin and valley polarization lifetime [26], give rise to valley-controlled spin-dependent features [13], and even produce magnetoelectric effects [27].

Here, it should be noticed that the role of the Hg lattice in jacutingaite family is of special interest because it is linked to the tunability of the properties hosted by these $(Pt/Pd)_2HgSe_3$ layers against external stimuli such as a vertical electric field.

Although jacutingaite is a family of ternary materials having many differences with the Xene family (graphene, silicene, etc.). However, the Hg atoms in this family form a buckled-type honeycomb structure similar to the Xene family.

Additionally, after the Pt atoms with dominant contribution around the Fermi level, the next significant contribution in the band structure originates from the Hg atoms. Thus because of the characteristics like buckling-type honeycomb geometry of the Hg lattice, high spin-orbit coupling effects, and the significant role of the Hg atoms around the Fermi surface, the properties of the $(Pt/Pd)_2HgSe_3$ layers can be easily modified by exposing them to a vertical electric field. In this context, we employ the vertical electric field as an external stimulus to break the inversion symmetry in the $(Pt/Pd)_2HgSe_3$ layers. The electric field in two-dimensional solids can be, in principle, controlled by electrostatic gating techniques. Here, we wish to mention that, overall, we employ three different strategies to exploit the inversion symmetry in the jacutingaite family: exposing to a vertical electric field, interfacing differ-

ent layers in this family using the heterobilayer approach, and finally growing on a ferroelectric substrate with switchable electric polarization to explore the effects of the induced electric field. Using these strategies, we realize many interesting phenomena based on the inversion symmetry breaking principle in the jacutingaite family.

Specifically, we notice the following: (i) The low-energy carriers in the jacutingaite family experience an effective valley Zeeman spin-orbit coupling that is entirely gated tunable to the extent that it can be switched on or off by a vertical electric field. In particular, two types of spin-orbit coupling appear when inversion symmetry is broken in the jacutingaite family, one is the so-called in-plane spin-orbit coupling of the Rashba type where spins are in-plane polarized. Another is the so-called Ising spin-orbit coupling, which points in the out-of-plane direction with an opposite sign at the opposite valleys, commonly known as valley-Zeeman spin-orbit coupling. The coexistence of in-plane and out-of-plane spin-orbit coupling brings a unique type spin texture as previously observed in single-layer graphene [28] and bilayer graphene [29] grown over transition metal dichalcogenides. However, the small band gap and low spin-orbit coupling in these heterostructures limit their applications to a low-temperature scale. And in this context, the jacutingaite family could be more suitable for such phenomena due to high spin-orbit coupling, more significant nontrivial band gap at the Fermi surface, and free from hurdles as used to enhance spin-orbit coupling via adatoms or heterostructures approach in graphene-based systems. (ii) The QVH and QSH effects emerge simultaneously where the spin and valley indices of the carriers can be switched with the application of electric field or gating the Pt_2HgSe_3 layer. (iii) Broken inversion symmetry with strong spin-orbit coupling makes the valley-dependent optical selection rule spin dependent, and carriers with several unions of the valley and spin indices can be selectively stimulated by optical fields with left- and right-handed circular polarization. (iv) Inversion asymmetry in the jacutingaite family introduces the spin-valley locking and electric switchable valley spin polarization that establishes a robust platform for realizing phenomena like the valley spin-valve effect. For the valley spin-valve effect, spin-valley locking and their switching by electric field or gating are the essential ingredients. Remarkably, the valley spin polarization in the jacutingaite family can be switched by an external electric field, which facilitates functionalities of a valley-spin polarizer or a valley-spin analyzer where the spin-valley transport can be ON or OFF depending on the polarity of the applied electrostatic gating. (v) Spin-polarized constant energy contours with triangular and star-like shapes near the Fermi surface are observed, indicating highly trigonal warping behavior in the jacutingaite family. (vi) By breaking the inversion symmetry in the jacutingaite family via growing the composite of Pt_2HgSe_3 and Pd_2HgSe_3 layers, the phenomena including valley contrasting Berry curvature, valley/layer selective optical absorption, layer crossover accompanied by spin crossover in the valence bands, and inverting the spin-valley characters with the application of electric field, are observed. We also observe the Rashba spin splitting around the low symmetric M point where the states are usually less influenced by breaking the inversion asymmetry due to its low-symmetric nature than the Γ point. (vii) By applying

TABLE I. Description of the existing crystallographic symmetries in the jacutingaite family and effect of vertical electric field upon them.

$(Pt/Pd)_2HgSe_3$	Point group	C_{3z}	C_{2x}	I	S_{6z}	M_{yz}
Pristine	D_{3d}	yes	yes	yes	yes	yes
E_z	C_{3v}	yes	no	no	no	yes

electric field through interfacial coupling with ferroelectric $III_2 - VI_3$ film (taken Al_2S_3 as an example) with bistability, high spin splitting ($\sim$188 and 120 meV in the lowermost conduction and topmost valence bands, respectively), spin-valley locking and QVH effect with large global band gap are observed in the Pt_2HgSe_3 layer. Moreover, the location of the chemical potential and band gaps can be controlled by changing the polarization state of the ferroelectric Al_2S_3 from $+P$ to $-P$. For instance, Pt_2HgSe_3 layer becomes hole-doped ($\sim$0.3 holes) when the polarization state of the Al_2S_3 shifts from $+P$ to $-P$. (viii) Finally, the realization of valley Hall and spin-valley Hall kink states are proposed in the jacutingaite family.

In this paper, calculations are carried out using the first principle approach as implemented in the Vienna *ab initio* simulation package [30,31]. Topological properties such as Berry curvatures $\Omega_z(k)$, topological $\mathcal{Z}_2$ invariant and surface states are calculated using the algorithm discussed in

Refs. [32–34]. Simulation methods are described with more detail in the Supplemental Material (SM) [35].

II. COEXISTENCE OF QUANTUM SPIN/VALLEY HALL EFFECTS

The point group of the $(Pt/Pd)_2HgSe_3$ monolayer is D_{3d}, which preserves the inversion symmetry arises from the combination of rotational and reflection symmetries in the system. This inversion symmetry can be broken by exposing $(Pt/Pd)_2HgSe_3$ monolayers to a transverse electric field [see Table I and Fig. 1] or possibly interfacing with other systems from the same or different families. We consider Pt_2HgSe_3 layer as an example to demonstrate our findings.

In the absence of spin-orbit coupling effects, the freestanding Pt_2HgSe_3 layer is semimetallic where the conduction and valence bands meet around special points in Brillouin zone (K_+ and K_-) at the Fermi surface in a similar way as in Xene solids. Also, the spin-up and spin-down bands are degenerated [see Figs. 1(a) and 1(b)]. By switching on the spin-orbit coupling effects, the massless Dirac type behavior becomes to massive one with a large band gap ($\sim$149 meV at Perdew-Burke-Ernzerhof level) and Pt_2HgSe_3 layer convert into a Kane-Male topological phase [see Figs. 1(d) and 1(e)]. However, the spin-up and spin-down bands are still degenerated [see Fig. 1(e)] due to the inversion symmetry in the layer. By calculating the Berry curvature, we obtain $\Omega_z(k) = 0$, which is expected due to the simultaneous
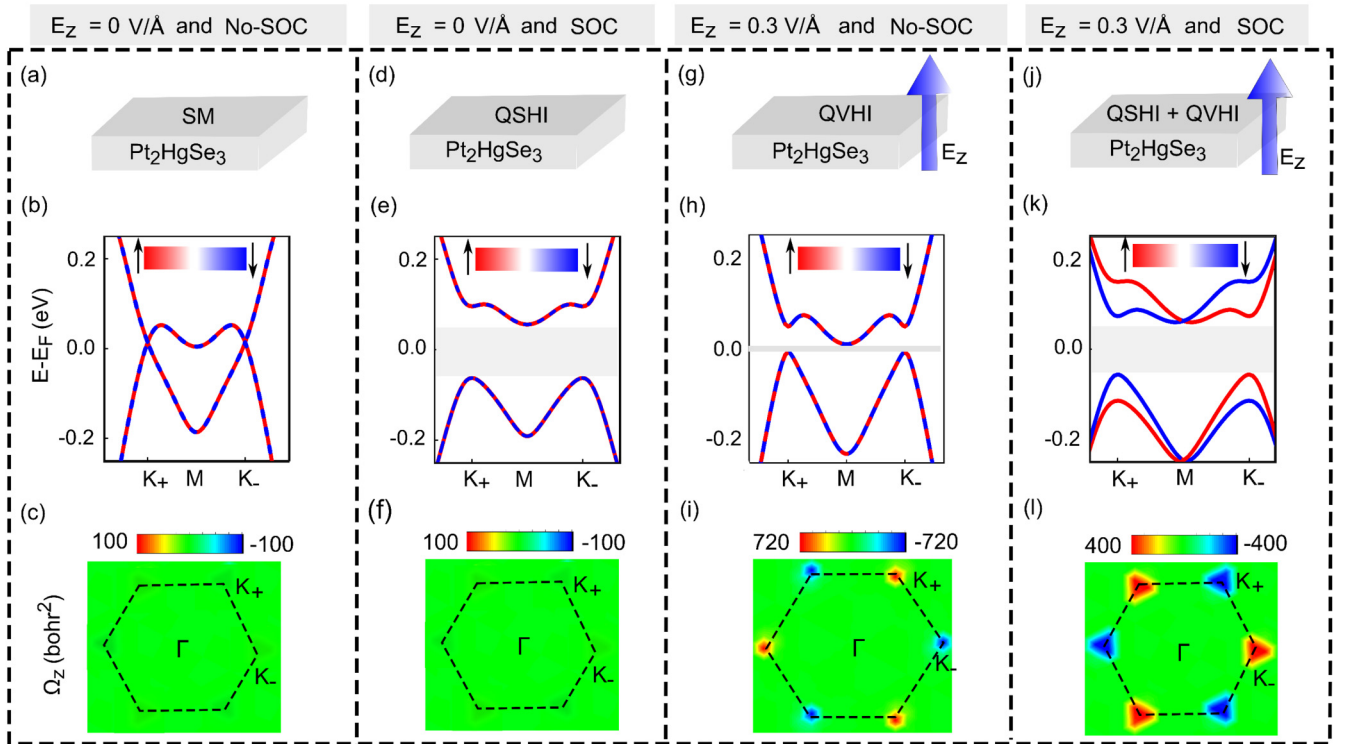

FIG. 1. Evolution of the energy spectrum and Berry Curvature of Pt_2HgSe_3 layer by switching ON/OFF the transverse electric field E_z and spin-orbit coupling effects. [(a)–(c)] Both spin-orbit coupling and electric field are switched off. [(d)-(f)] E_z is switched off, but spin-orbit coupling is switched on. [(g)–(i)] E_z is switched on, but spin-orbit coupling is switched off. [(j)–(l)] Both E_z and spin-orbit coupling are switched on. Inside the figures, SM, QS(V)HI, and SOC stand for semimetal, quantum spin (valley) Hall insulator, and spin-orbit coupling, respectively.

presence of both time-reversal and space inversion symmetries [see Fig. 1(f)]. Similarly, by exposing the Pt_2HgSe_3 layer to the external transverse electric field without including the spin-orbit coupling effects [see Fig. 1(g)], the Pt_2HgSe_3 layer turns to the QVH phase with a band gap ($\sim$13.6 meV) at the Fermi surface [see Fig. 1(h)]. However, the spin-up and spin-down bands are overlapped due to the absence of spin-orbit coupling effects [see Fig. 1(h)]. Due to the broken inversion symmetry in the system, we obtain valley contrasting Berry curvature for valley K_+ and K_- [see Fig. 1(i)] confirming the QVH anomaly in the Pt_2HgSe_3 layer.

When both electric field and spin-orbit coupling are switched-on simultaneously [see Fig. 1(j)], we notice the spin polarization where spin-up and spin-down bands are not overlapping anymore [see Fig. 1(k)], and the system has a peculiar spin-valley coupling. In addition, the global band gap further enlarges ($\sim$93 meV) when the spin-orbit coupling is switched-on in the presence of a finite electric field. Further, by measuring the $\mathcal{Z}_2$ topological number and surface states, we find that the simultaneous presence of both spin-orbit coupling and electric field does not hurt the $\mathcal{Z}_2$ topological signatures in the system, and Pt_2HgSe_3 layer is still a QSH insulator as it is before the application of electric field. However, this time, it also displays the valley contrasting Berry curvature where it shows opposite peaks for opposite valleys [see Fig. 1(l)] signifying QVH insulating phase in the Pt_2HgSe_3 layer. This shows that both the twins QSH and QVH effects emerge simultaneously in the Pt_2HgSe_3 layer; we call it coupled spin-valley Hall effects or quantum spin-valley Hall effect. Thus, the jacutingaite family could remarkably establish a suitable platform to bring QSH and QVH phenomena into a single real material. The spin-orbit coupling, together with electric field, lifts the spin degeneracy of energy bands and marks the system for having spin-valley coupling.

III. ELECTRIC FIELD SWITCHING EFFECTS

Here, we ask the question: Is it possible to invert or reverse the spin polarization at the valley points or role of valleys by reversing the orientation of the electric field from $E_z > 0$ to $E_z < 0$? We calculate the spin polarization at the two valleys in the $E_z > 0$ and $E_z < 0$ states to systematically address this question. Interestingly, we find that it is indeed possible to switch or interchange valley K_+ and K_- by turning the direction of the electric field from $E_z > 0$ to $E_z < 0$ [see Fig. 2]. For instance, the spin order in the energy bands at valley K_+ (K_-) shifts to valley K_- (K_+) by switching electric field from $E_z < 0$ to $E_z > 0$ [see Figs. 2(b) and 2(e)], indicating electrically switching response of valley and spin polarization. The spin splitting size in the lowermost conduction and topmost valence bands reach around $\sim$62 and 48 meV, respectively, when the Pt_2HgSe_3 layer is subjected to an electric field with strength $E_z = \pm 0.3$ V/Å [see Fig. 2(c)]. This sizable spin splitting is fully reversible by switching the direction of the electric field from $E_z > 0$ to $E_z < 0$ [see Figs. 2(c) and 2(f)]. In principle, turning the sign of E_z from $E_z > 0$ to $E_z < 0$ is equivalent to the inversion symmetry operation, which changes the momentum K_+ (K_-) to K_- (K_+) while the spin rests invariant. As controlled by the electric field, the spin-valley locking is important for effects like spin valve
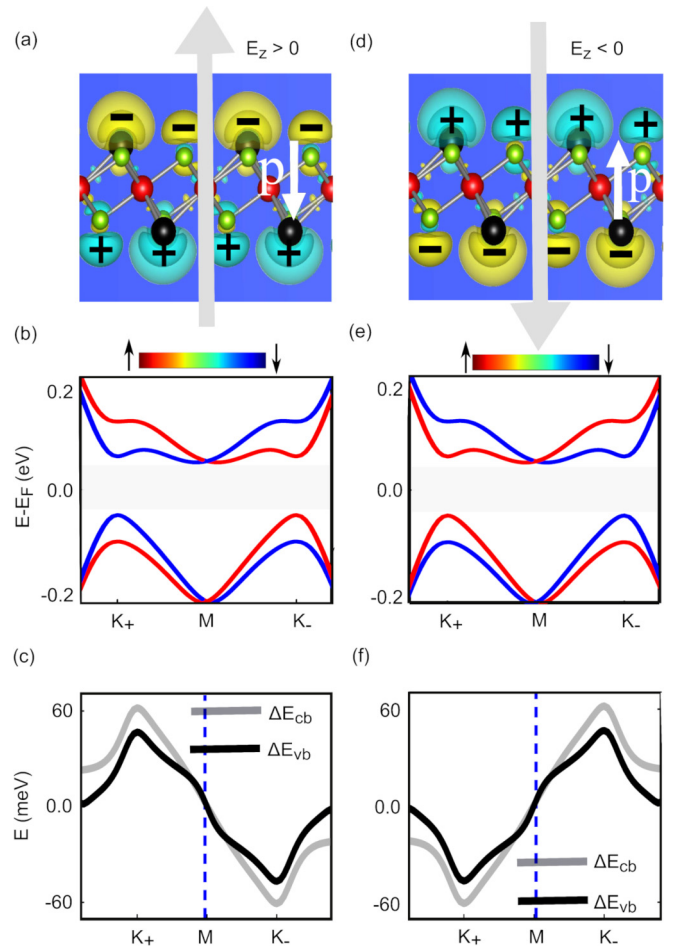

FIG. 2. (a) Differential Charge density $\rho[\equiv \rho(E_z = 0.0) - \rho(E_z = +0.3)]$ of the Pt_2HgSe_3 layer. The yellow and cyon colors represent the charge accumulation and depletion. The vector p represents the induced polarization. (b) The spin-resolved band structure of the Pt_2HgSe_3 layer exposed to a vertical electric field $E_z > 0$ ($E_z = +0.3$ V/Å). (c) The size of the spin splitting in the lower conduction [$\Delta E_{cb} \equiv E_\uparrow - E_\downarrow$] and top valence bands [$\Delta E_{vb} \equiv E_\uparrow - E_\downarrow$]. [(d),(e)] Representing the same meaning as [(a)–(c)] but here the electric field is oriented along the $-z$ direction, i.e., $Ez < 0$ ($E_z = -0.3$ V/Å).

and valley spin-valve effects. As evident from the differential charge density analysis, turning E_z from $E_z > 0$ to $E_z < 0$ shifts free electronic charge density to the top Hg-Se layers and vice versa [see Figs. 2(a) and 2(d)]. The shifting of the charge density by E_z induces polarization in the Pt_2HgSe_3 layer, which is reversible by the electric field.

Remarkably, by reversing the sign of the electric field from $E_z > 0$ to $E_z < 0$, the $\mathcal{Z}_2$ topological invariant remain unchanged (i.e., $\mathcal{Z}_2 = 1$) whereas the Berry curvatures $\Omega_z(K_+)$ and $\Omega_z(K_-)$ are interchanged [see Fig. 6]. Alternatively, we notice a trend, $\Omega_z(E_z > 0, \tau_z) \approx -\Omega_z(E_z < 0, \tau_z)$, in the jacutingaite family, where τ_z represents the valley index. Furthermore, it can be seen from Figs. 3(a)–3(f), the surface states are coupled to the direction of the electric field and can be potentially controlled by swapping the direction of the electric field from $E_z > 0$ to $E_z < 0$. For instance, for the $E_z > 0$ case, the surface states connect the V_{tvb} and $C_{lcb} + 1$ bulk
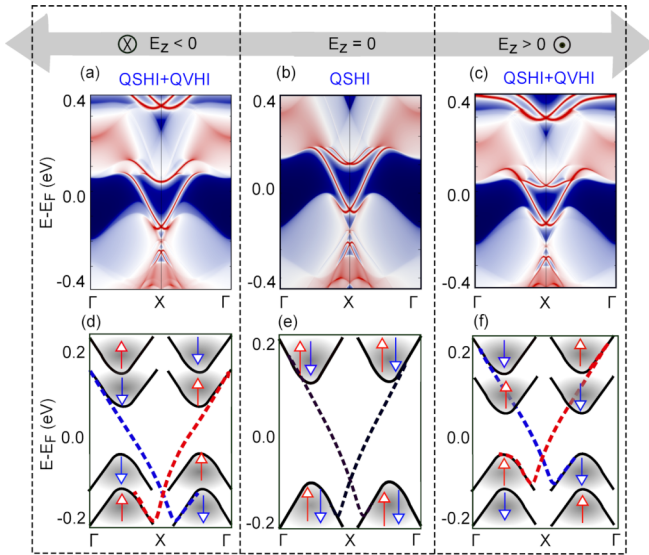
FIG. 3. [(a)–(c)] surface states of the Pt_2HgSe_3 layer for the cases: (a) $E_z < 0$ ($E_z = -0.3$ V/Å), (b) $E_z = 0$ V/Å and (c) $E_z > 0$ ($E_z = +0.3$ V/Å). [(d)–(f)] Schematic representation describing the effects of electric field orientation on the edge states for the (d) $E_z < 0$, (e) $E_z = 0$, and (f) $E_z > 0$ cases.

bands while it connecting the $V_{tvb} - 1$ to C_{lcb} bands for the $E_z < 0$ case, V_{tvb} (C_{lcb}) represents the topmost valence band (lowermost conduction band).

Due to the spin-valley coupling, the optical transition between the V_{tvb} and C_{lcb} bands driven by circularly polarized light strongly depends on the spin, valley and light handedness (such as left-handed or right-handed). To evaluate the optical interband transition by circularly polarized light, we estimate the quantity $\eta^{(s)}(k)$, which represents the spin-dependent degree of circular polarization between the V_{tvb} and C_{lcb} bands, and is defined as $\eta^{(s)}(k) = (1/N)|P_+^{(s)}(k)|^2 - (1/N)|P_-^{(s)}(k)|^2$, where $N = |P_+^{(s)}(k)|^2 + |P_-^{(s)}(k)|^2$ [36]. Here, $P_\pm^{(s)}(k)$ represent the interband matrix elements for the left ($-$) and right ($+$) handed circularly polarized light at a given spin s and k, and are defined as $P_\pm^{(s)}(k; n, n') = \langle n'k, s|p_x \pm ip_y|nk, s\rangle$, where n

FIG. 5. [(a)–(c)] Constant energy contours maps at ($E = E_F - 0.106$ eV) describing the two-dimensional spin texture and Fermi surface topology along various spin components S_x, S_y, and S_z for the $E_z > 0$ ($E_z = +0.3$ V/Å) case. [(d)–(f)] The same as described in (a)–(c) but for $E_z < 0$ ($E_z = -0.3$ V/Å) case. The trigonal type effects and switching of the spin texture by inverting the electric field direction can be noticed.
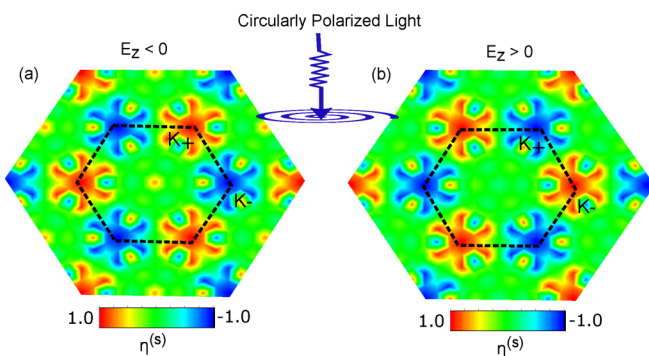

FIG. 4. Valley driven circular dichroism distribution maps describing the selective optical interband transition $\eta_s(k)$ for the right-handed circularly polarized light for (a) $E_z > 0$ and (b) $E_z < 0$ cases. For left-handed circularly polarized light, the role of valley K_+ and K_- become inverted (not shown here).
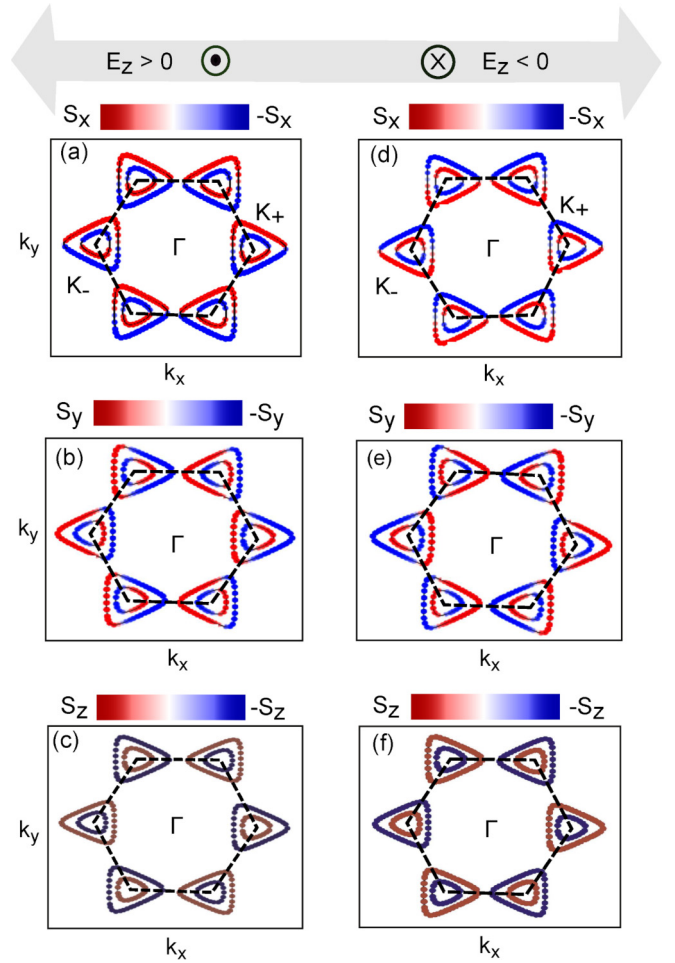
and n' represent the bands involved in the transition process. The value of $\eta^{(s)}(k)$ estimates the relative absorption rates of left and right-handed circularly polarized light photons. In the above relation, we assume that the spin-flip transitions are absent in the optical processes. As shown in Figs. 4(a) and 4(b), single layer Pt_2HgSe_3 having perfect circular dichroism in the vicinity of K_+ and K_-, which is valley dependent and selectively decays as one moves away from the valley points. For instance, for the $E_z > 0$ case, valley K_+ with spin-up is excited while the opposite valley is frozen to participate in the optical transition for right-handed circularly polarized light. Changing the light handedness (such as from left to right or vice versa) or switching the vertical electric field sign can selectively freeze/allow the optical transition between the V_{tvb} and C_{lcb} bands. Remarkably, the swapping of interband transition between the two valleys is possible by inverting the direction of the electric field [see Figs. 4(a) and 4(b)]. This allows the valley-dependent interplay of the carrier with circularly polarized light.
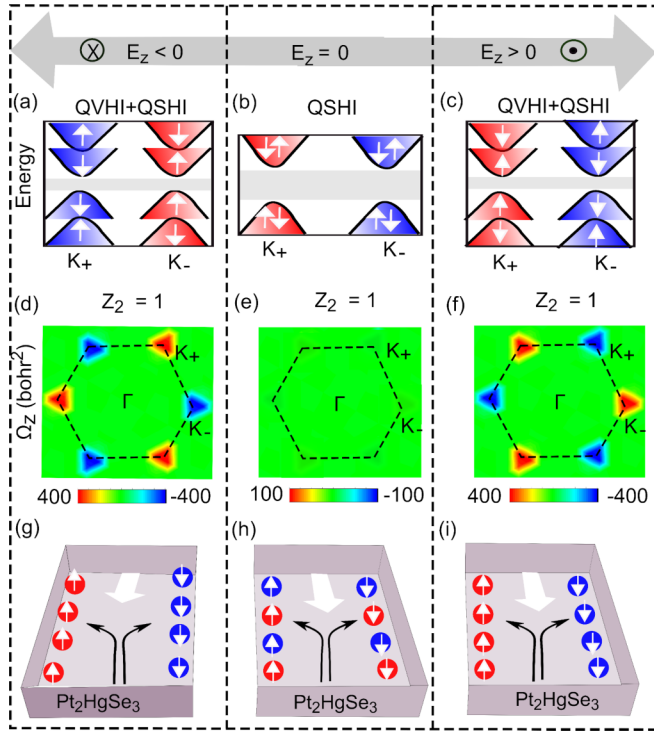
FIG. 6. [(a)–(c)] Schematics of spin-resolved low-energy band structures around valley K_+ and K_- for the cases (a) $E_z < 0$ ($E_z = -0.3$ V/Å), (b) $E_z = 0$ V/Å, and (c) $E_z > 0$ ($E_z = +0.3$ V/Å). Bands shaded in red and blue color represent the valley K_+ and K_-, respectively. [(d),(e)] Berry curvature distribution maps over the Brillouin zone for the cases (d) $E_z < 0$ ($E_z = -0.3$ V/Å), (e) $E_z = 0$ V/Å, and (f) $E_z > 0$ ($E_z = +0.3$ V/Å). $\Omega_z(E_z > 0, \tau_z) \approx -\Omega_z(E_z < 0, \tau_z)$ trend can be noticed. [(g)–(i)] Schematic representation of coupled QSH and QVH effects, and QSH effect (h). The blue and red solid spheres represent the carriers corresponding to valley K_+ and K_-, respectively.
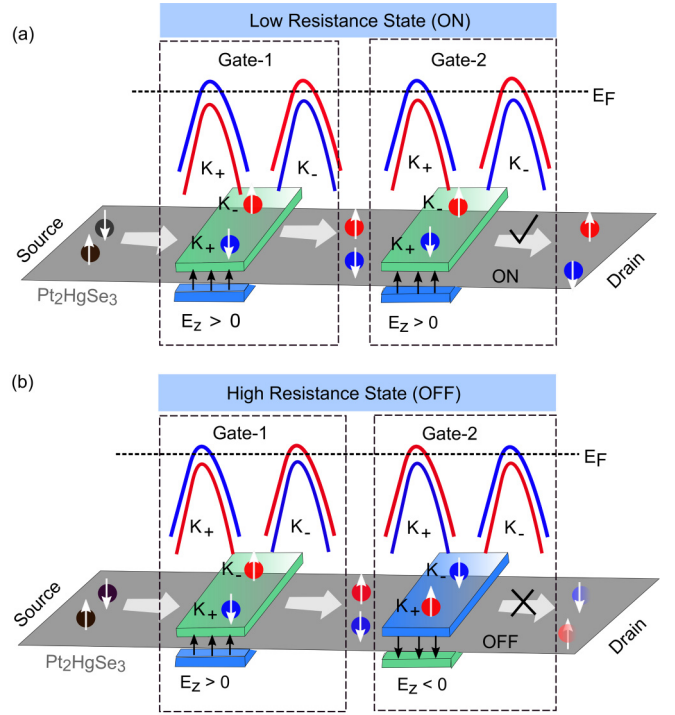

FIG. 7. Schematic representation describing the working principle of the valley spin-valve effect. (a) Parallel combination: The applied electric fields generated by the gate voltage in region-1 (act as a spin-valley polarizer) and region-2 (act as a spin-valley analyzer) are parallel. (b) Antiparallel combination: Same as described in (a) but for opposite electric fields in region-1 and region-2. The ON/OFF state depends on the relative orientation of the applied electric fields in region-1 and and region-2. The red and blue spheres represent the carriers belong to valley K_+ and K_-, respectively. Similarly, the red and blue solid curves represent the spin-up and spin-down states, respectively. The vertical dotted-line rectangles in (a–b) correspond to Region-1 and Region-2, respectively.

IV. VALLEY SPIN-ORBITAL EFFECTS

We further analyze what type of spin splitting induces in the Pt$_2$HgSe$_3$ layer when exposed to an electric field. For this purpose, we plot spin-resolved band structures where different spin components (such as S_x, S_y and S_z) are shown (see Fig. S2 in SM [35]). As can be noticed from Fig. S2 in SM [35], the calculated spin expectation values for the low-energy states are principally distributed both in the out-of-plane and in-plane of the sample. The most dominant contribution of spin polarization originates from the out-of-plane spin component S_z, whereas the in-plane spin components S_x and S_y are moderately nonzero. This unique type of spin texture where both in-plane and out-of-plane spin contribution exist has been previously observed in WSe$_2$/bilayer − graphene heterostructure [29]. In principle, two types of spin-orbit coupling appear when inversion symmetry is broken in the jacutingaite family, one is the so-called in-plane spin-orbit coupling of the Rashba type, which pins carrier spins to the in-plane directions with helical spin textures while another is the so-called Ising spin-orbit coupling, which pins carrier spin to the out-of-plane direction with an opposite sign at the opposite valleys and is commonly known as valley-Zeeman spin-orbit

coupling. The coexistence of Ising and Rashba spin-orbit couplings in the gated jacutingaite family results in a unique spin texture that can be swapped by changing the electric voltage polarity.

We further calculate the constant energy contour maps in the momentum space along different spin components (S_x, S_y, and S_z) to visualize the spin texture around the valley points and Fermi surface morphology (see Fig. 5). We notice that the constant energy contours have different shapes around different high symmetry k points in the Brillouin zone. For instance, in the vicinity of the valley points (K_+ and K_-), we observe triangular-type shaped contours, indicating a hexagonal warping character (see Fig. 5 and SM [35]) in the jacutingaite family. In order to have a look at the possibility of switching the spin texture and spin or valley characters, we invert the electric field from $E_z > 0$ to $E_z < 0$. Interestingly, by reversing the direction of the electric field, the spin texture of the inner and outer branches are reversed simultaneously as illustrated in Fig. 5, indicating the full electric controllability of spin states in the Pt$_2$HgSe$_3$ layer (see Fig. 5). The Fermi surface topology and constant energy contour analysis of the Pd$_2$HgSe$_3$ is discussed in the SM [35].
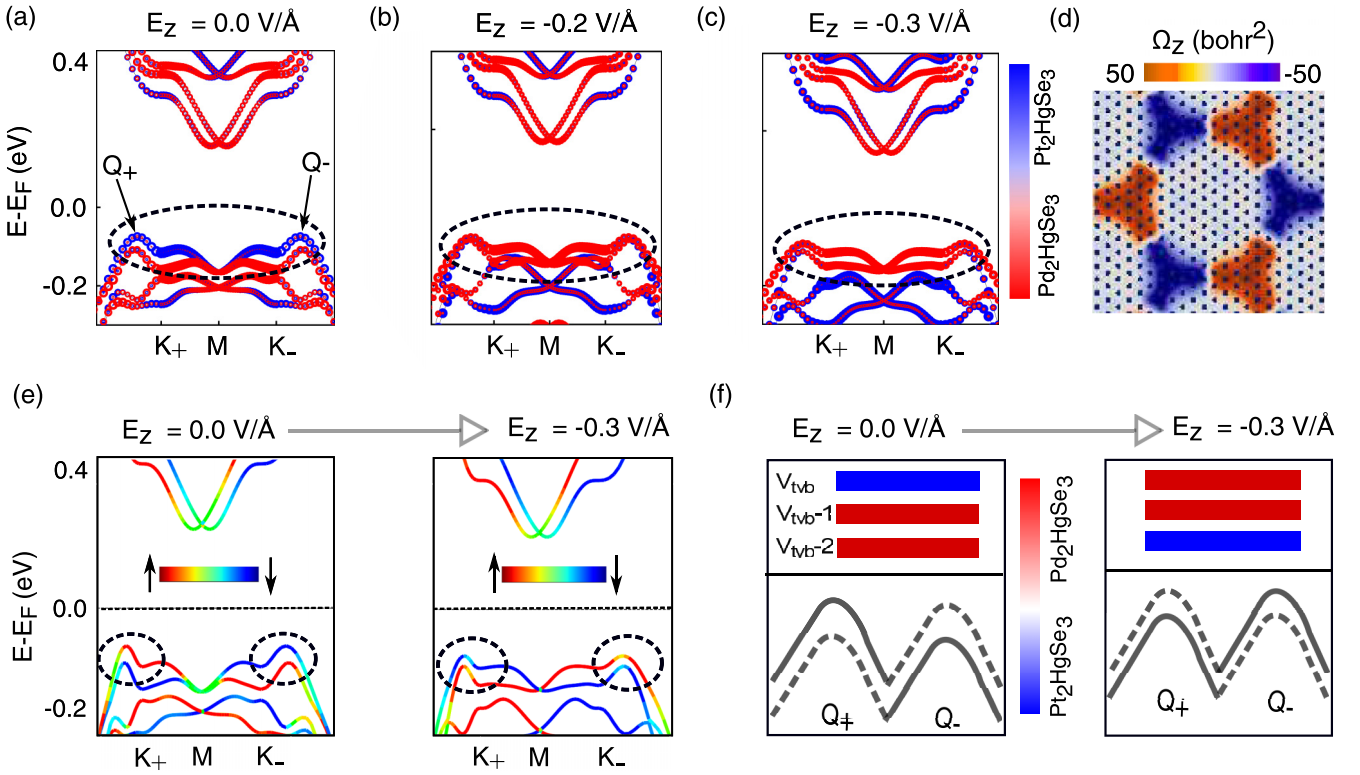
FIG. 8. [(a)–(c)]: Layer resolved band structures of the Pt_2HgSe_3/Pd_2HgSe_3 heterobilayer with spin-orbit coupling effects included for the $E_z = 0$ V/Å (a), $E_z = -0.2$ V/Å (b) and $E_z = -0.3$ V/Å (c) cases. The crossover between the states stemmed from Pt_2HgSe_3 and Pd_2HgSe_3 layers driven by an electric field oriented along the $-z$ direction can be noticed. (d) The distribution of the Berry curvature over the first Brillouin zone in the absence of an electric field. (e) The spin-resolved band structure of the Pt_2HgSe_3/Pd_2HgSe_3 system for the $E_z = 0$ V/Å (a) and $E_z = -0.3$ V/Å (b) cases. (f) A schematic representation reflecting the layer crossover (top section) and spin crossover (bottom section) driven by an electric field oriented along the $-z$ direction. The solid/dashed black curve represents the spin-up/spin-down bands and $V_{tvb} - i$ (with $i = 1, 2$) represent the topmost three valence bands around the valley points Q_+/Q_-, respectively.

V. SWAPPING OF SPIN VALLEY CURRENTS BY SWITCHING ELECTRIC FIELD DIRECTION

It can be seen that the turning of the electric field from $E_z > 0$ to $E_z < 0$ inverts the Berry curvature peaks at the valley K_+ and K_- [see Figs. 6(d) and 6(f)], meaning that the effective magnetic field is reversed. The direction reversal of the Berry curvature affects the carrier deflection with respect to spin and valley indices, as shown by the schematic diagram [see Figs. 6(g) and 6(i)]. As can be seen that there is a spin-Hall current and a valley-Hall current. In particular, for the $E_z > 0$ case, spin-up (spin-down) electrons from the valley K_+ (K_-) accumulate on one boundary (opposite boundary) [Fig. 6(i)]. Thus, each boundary drags a net spin polarization as well as a net valley polarization while electrically remains neutral with no charge current. By turning electric field to $E_z < 0$, the above scenario reverses. Thus by turning the electric field, we can swap spin and valley currents [see Figs. 6(g) and 6(i)].

VI. VALLEY SPIN-VALVE EFFECTS

As shown above, the spin valley polarization in Pt_2HgSe_3 layer is coupled with the electric field—it can be switched ON or OFF by changing the direction of E_z; this behavior supports functionalities of a valley spin polarizer or a valley spin analyzer. By adjusting the Fermi level in the conduction

or valence band, one can design a functional device working on the principle of the so-called valley spin-valve effect where conductance can be switched to an ON or OFF state that depends on the relative valley-spin polarization established by the polarizer and the analyzer. The way the valley spin-valve effect can work in a device form is presented schematically in Fig. 7. The incoming electrons with no spin and valley polarization are injected from the metallic source, which becomes spin and valley polarized when entering the region-1 (acting as a spin polarizer), where the electric field is applied in the $+z$ direction [see Fig. 7(a)]. After passing through region-1, electrons are spin-up (spin-down) polarized in valley K_+ (K_-), and it is because of spin-valley locking, which is induced due to inversion symmetry breaking by electric field. These spin and valley polarized electrons now enter the region-2 (acting as an analyzer), where the electric field is applied again in the $+z$ direction [see Fig. 7(a)]. Now, if the applied electric field is parallel to that in region-1, the electrons of both spin-up and spin-down components are allowed to be efficiently transmitted through the intravalley transport [see Fig. 7(a)]. This is called the ON state or low resistance state. In contrast, if the applied electric field is anti-parallel to that in region-1, the spin-up and spin-down electrons are not allowed to transmit from region-2 [see Fig. 7(b)]. This is called the OFF state or high resistance state. In this way, the valley spin-valve device switches the resistance from low to high and vice versa.
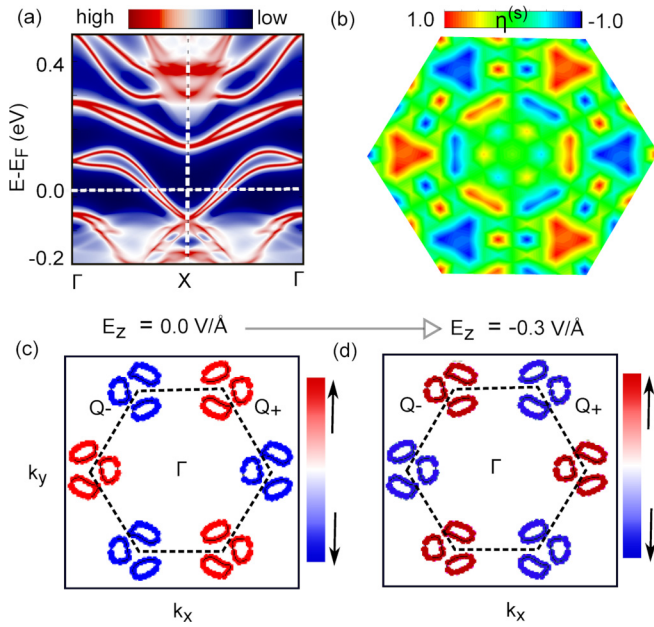
FIG. 9. Surface states for the side surface (right surface) of the Pt_2HgSe_3/Pd_2HgSe_3 heterobilayer. (b) Valley-driven circular dichroism distribution maps over the first Brillouin zone between the V_{tvb} and C_{lcb} bands for right-handed circularly polarized light. Spin-resolved constant energy contours maps at $E = E_F - 0.095$ eV, reflecting the spin texture and morphology of the bands near to the Fermi level for $E_z = 0$ V/Å (c) and $E_z = -0.3$ V/Å (d).

VII. LAYER AND SPIN CROSSOVER IN Pt_2HgSe_3/Pd_2HgSe_3 HETEROBILAYER

As an alternative way to break the inversion symmetry and introduce staggered type potential, we interface Pt_2HgSe_3 with the Pd_2HgSe_3 layer in the form of heterobilayers (see the atomic structure from Fig. S4 in SM [35]). Due to the built-in electric field established by the interfacial coupling, strong spin-valley coupling is induced. A large global band gap $\sim$231 meV is opened after establishing the interfacial coupling between Pt_2HgSe_3 and Pd_2HgSe_3 layers. However, the valleys in the Pt_2HgSe_3/Pd_2HgSe_3 heterobilayer are shifted from the K_+/K_- points to other very-nearby k points labeled as Q_+/Q_-, and we may call it Q_+/Q_- valleys [see Figs. 8(a)–8(c)]. The layer resolved band structure shows that the V_{tvb} band originate from the Pt_2HgSe_3 layer while $V_{tvb} - 1$ and $V_{tvb} - 2$ originate from the Pd_2HgSe_3 layer [see Fig. 8(a)]. Additionally, the spin-resolved band structure [see Fig. 8(e)] shows that the spin polarization is strongly valley dependent indicating a robust spin-valley locking. Thus the Pt_2HgSe_3/Pd_2HgSe_3 heterobilyer establishes a rich platform where spin, valley, and layer degrees of freedom combined.

By applying an electric field in the $-z$ direction, we observe a spin crossover between the two valleys, which is accompanied by layer crossover [see Figs. 8(a)–8(c) and 8(e)–8(f)]. By increasing the strength of the electric field from zero to negative, the spin order at two valleys and layer order (from Pt_2HgSe_3 to Pd_2HgSe_3) finally switches when $E_z \sim -0.3$ V/Å. After the layer crossover, the topmost valence band V_{tvb} is now stemming from the Pd_2HgSe_3 layer

instead of Pt_2HgSe_3 layer. To our knowledge, such type behavior where layer, spin and valley crossovers occur is very rare.

Due to valley contrasting Berry curvature [see Fig. 8(d)], Pt_2HgSe_3/Pd_2HgSe_3 heterobilayer shows QVH signature together with valley selective optical interband transition (circular dichroism) when exposed to circularly polarized light [see Fig. 9(b)]. By examining the topological signature in Pt_2HgSe_3/Pd_2HgSe_3 heterobilayer via calculating the $\mathcal{Z}_2$ topological invariant, we find $\mathcal{Z}_2 = 0$ showing that it is a trivial band insulator. However, there exist surface states at the Fermi surface [see Fig. 9(a)]. Apparently, these surface states have an analogous resemblance with the bands splitted through Rashba spin-orbit coupling. We may call the Pt_2HgSe_3/Pd_2HgSe_3 system a QVH insulator with Rashba-like splitted edge states. By examining the constant energy contours near the Fermi level, we observe elliptical-type shaped contours reflecting a trigonal warping distortion around the valley points [see the color map plots in the k_x and k_y momentum plane in Figs. 9(c) and 9(d)], which is completely switchable by electric field inversion.

VIII. RASHBA SPIN SPLITTING AROUND THE M POINT

Furthermore, we notice a Rashba spin splitting in the lower conduction bands around the M point in the Brillouin zone, see Figs. S5(a)–S5(c) in SM [35], where the most dominant contribution of spin polarization is coming from the the in-plane spin components S_x and S_y while the out-of-plane spin component S_z is moderately nonzero. The size of the Rashba splitting between C_{lcb} and $C_{lcb} + 1$ bands is estimated to be $E_R = 9.7$ meV, and the momentum offset is estimated to $k_0 = 0.037$ Å^{-1}. To estimate the Rashba coefficient α_R, we use $\alpha_R = 2E_R/k_0$. We find $\alpha_R = 524$ meV Å^{-1} in Pt_2HgSe_3/Pd_2HgSe_3 system. Normally, the bands around the M point are usually less affected in the context of Rashba spin splitting as compared to the Γ point, when inversion symmetry is broken. It is because the M is a less symmetric point than Γ point in the Brillouin zone. Thus, solids with Rashba spin splitting around the M point in the Brillouin zone are rare, and so far, it has been observed only in the $PtBi_2$ bulk system [37].

IX. $(Pt/Pd)_2HgSe_3$ LAYERS OVER FERROELECTRIC $III_2 - VI_3$ FILM

Besides the external electric field, coupling with ferroelectric insulators provide another way to induce an electric field in the jacutingaite family. In this context, choosing Al_2S_3 from the In_2Se_3 ferroelectric family [38] as an example of ferroelectric insulator, we grow the Pt_2HgSe_3 layer over the Al_2S_3 substrate. Al_2S_3 belongs to the ferroelectric family of In_2Se_3, which has been experimentally reported to be a room-temperature ferroelectric [39]. In principle, two polarization states are possible for the ferroelectric material denoted by $+P$ and $-P$ polarization. The energy bands and the size of the global band gap strongly depend on the polarization state [see Fig. 10(a)]. For instance, when Pt_2HgSe_3 layer is deposited over the Al_2S_3 in the $+P$ polarization state, labeled by Pt_2HgSe_3/Al_2S_3 $(+P)$, the inversion symmetry is broken
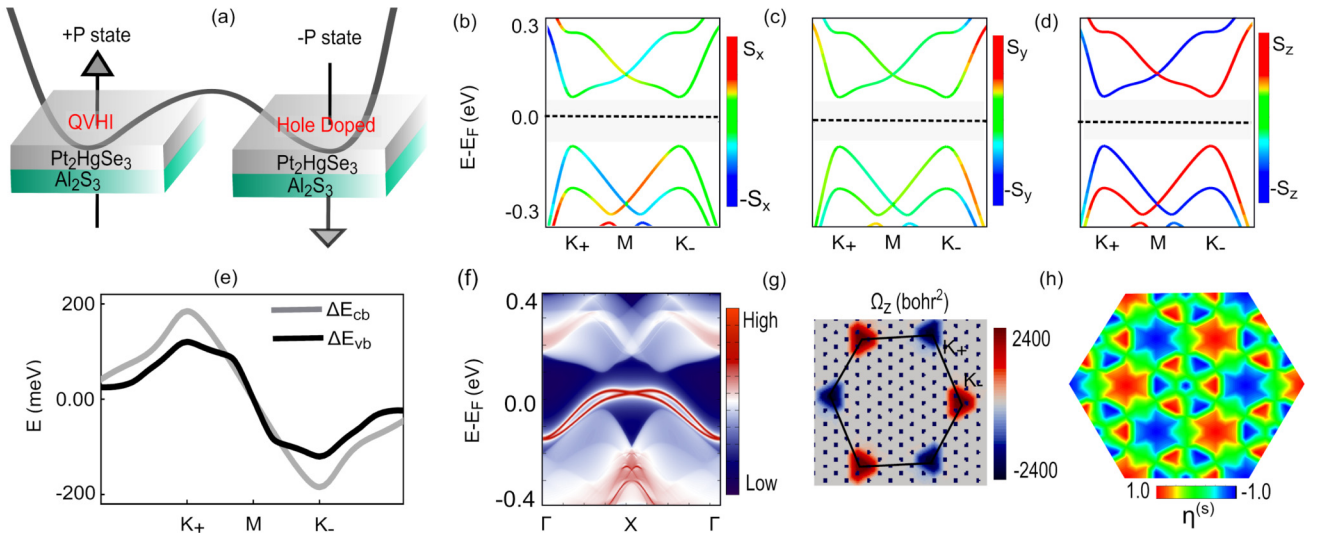
FIG. 10. (a) The schematic illustration describing the bistable phases of the Pt_2HgSe_3/Al_2S_3 system. The solid-black curve represents the energy curve. Whereas the vertical arrows symbolise the polarization state. [(b)–(d)]: The spin-resolved band structures of the Pt_2HgSe_3 layer grown over the ferroelectric $Al_2S_3(+P)$ layer for various spin components S_x (b), S_y (c), and S_z (d). The highly spin splitting in both valence and conduction bands can be noticed. (e) The size of the momentum dependent spin splitting in the top valence and lower conduction bands of the Pt_2HgSe_3 layer. (f) The surface states for the side surface (left surface) of the Pt_2HgSe_3 layer grown over the ferroelectric $Al_2S_3(+P)$ layer. (g) The distribution of the Berry curvature of $Pt_2HgSe_3/Al_2S_3(+P)$ heterobilayer over the momentum space. (h) Valley driven circular dichroism distribution maps over the momentum space between the V_{tvb} and C_{lcb} bands in the $+P$ polarization state for right-handed circularly polarized light.

in the Pt_2HgSe_3 layer, which is indeed the purpose of this paper. As a consequence, a direct band gap ($\sim$141 meV) is opened up at the valley points K_+ and K_- due to the combined efforts of induced polarization field and spin-orbit coupling [see Fig. 10]. The states around the Fermi level are mainly originated from the Pt_2HgSe_3 layer, whereas the states of Al_2S_3 are far beyond the Fermi level showing that Al_2S_3 could be a good substrate for the jacutingaite family. Moreover, by switching the spin-orbit coupling effects, the valence and conduction bands are largely splitted with opposite spin polarization at the opposite valleys indicating a strong spin-valley coupling in the Pt_2HgSe_3 layer [see Figs. 10(b)–10(e)]. We achieve the spin splitting with sizes reach to around $\sim$120 and 188 meV in the topmost valence and lowermost conduction bands, respectively. The Pt_2HgSe_3 layer becomes a QVH insulator after deposition over the $Al_2S_3(+P)$ layer due to displaying valley contrasting Berry curvature with an opposite sign at opposite valleys [see Fig. 10(g)].

To assess the topological identification of $Pt_2HgSe_3/Al_2S_3(+P)$ system, we calculate the $\mathcal{Z}_2$ topological number, which is zero ($\mathcal{Z}_2 = 0$). However, it is a valley Hall insulator due to opposite Berry curvature peaks at valley K_+ and K_-, that is $[\Omega_z(K_+/K_-) \gtrless 0]$.

Although in the $Pt_2HgSe_3/Al_2S_3(+P)$ heterobilayer there are no topologically protected edge states that connect the valence and conduction bands through the bulk band gap. Nonetheless, it has edge states, which originate from the bulk valence band and consequently pass through the Fermi surface without touching the bulk conduction band [see Fig. 10(f)].

We may call it a QVH insulator with Rashba-like splitted edge bands. What actually happens that Pt_2HgSe_3 system makes a phase transition from the $\mathcal{Z}_2$ nontrivial topological insulator to a trivial insulator (valley Hall insulator)

when deposited on the Al_2S_3 substrate? In principle, the Al_2S_3 substrate induces a staggered type spin-orbit coupling (valley-Zeeman) in the jacutingaite family, which may convert the $\mathcal{Z}_2$ nontrivial topological nature of the jacutingaite family to a trivial valley Hall state. Such behavior has also been previously reported for graphene-based systems deposited on transition metal dichalcogenides [40]. Because of the presence of valley-dependent Berry curvature, the $Pt_2HgSe_3/Al_2S_3(+P)$ heterobilayer is also suitable for valley selective optical interband absorption [see Fig. 10(h)].

Inspecting the spin resolved dispersions near the K_+ and K_- valleys, we observe that dominant contribution is coming from the out-of-plane spin component (S_z component) while the in-plane spin components are moderately nonzero [see Figs. 10(b)–10(d)]. This indicates the presence of both in-plane and out-of-plane spin contributions in the $Pt_2Hg_3Se_3/Al_2S_3$ system. Most importantly, by analyzing the constant energy contours near the Fermi surface, we observe triangular-like and star-like shaped contours in the top valence and lower conduction bands, respectively [see Fig. 11]. This indicates the presence of trigonal warping in the Pt_2HgSe_3 layer grown over the ferroelectric layer.

By switching the polarization state from $+P$ to $-P$, we find that the Fermi level shifts to the valence band of the Pt_2HgSe_3 layer, showing a charge transfer from the Pt_2HgSe_3 layer to the Al_2S_3 layer [see Fig. 12(b)]. The estimated shift of the Fermi energy (i.e., $E_v - E_F$) in the Pt_2HgSe_3 layer is around $\sim$82 meV, where E_c and E_F represent the top valence band edge and Fermi level, respectively. From this rigid shift of the Fermi level, we can approximately assess the apparent doping concentration in the Pt_2HgSe_3 layer, which is estimated to be $\sim$0.3 holes per unit cell in our case. Our findings hint to the possibility that tuning the polarization direction may be an
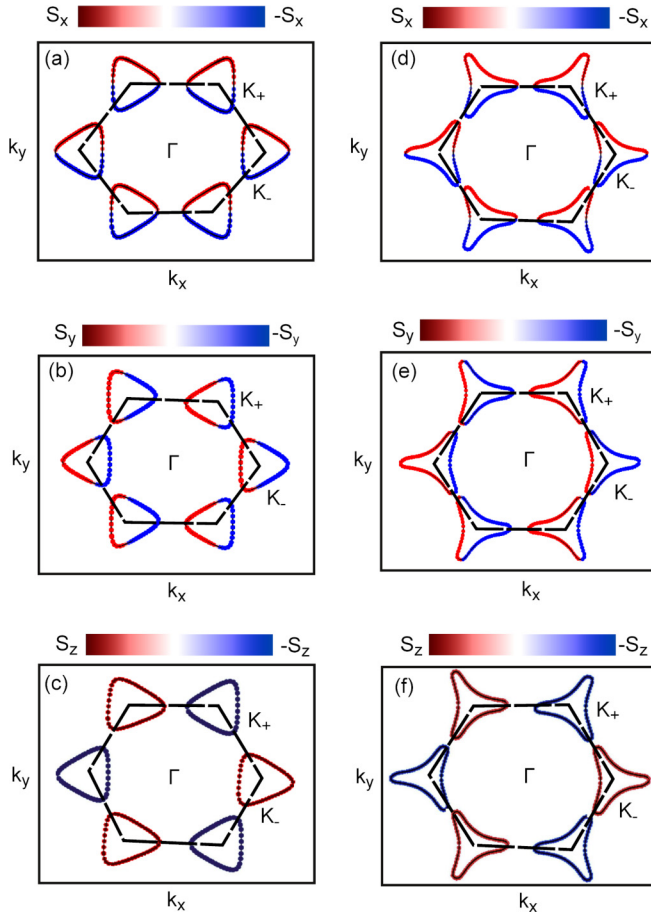
FIG. 11. Constant energy contours maps in the vicinity of the Fermi surface for various spin components S_x, S_y, and S_z in the $+P$ polarization state, describing the spin textures and shapes of the Fermi surface of Pt_2HgSe_3 layer grown over the ferroelectric Al_2S_3 layer. [(a)–(c)] Constant energy contours at the top valence bands ($E = E_F - 0.11$ eV). [(d)–(f)] Constant energy contours at the lower conduction bands($E = E_F + 0.15$ eV). The triangular and star-like shaped contours reflect the high trigonal distortion around the Fermi level of Pt_2HgSe_3 layer grown over the ferroelectric Al_2S_3 layer.

effective way to control the doping level in Pt_2HgSe_3 layer, similarly to quaternary topological insulators [41]. This may also lead to the possibility of unconventional superconductivity as predicted by the recent report in the jacutingaite family [42].

Thus, it is possible to tune the location of the Fermi level in the Pt_2HgSe_3 layer by turning the polarization direction of the ferroelectric layer from $+P$ to $-P$ [see Fig. 12]. This indeed allows significant control of the doping level in the jacutingaite family. In particular, the conduction band minimum of the Al_2S_3 is energetically lower than the valence band maximum of the Pt_2HgSe_3 layer in the–P polarization state, indicating an Ohmic contact between these two layers [see Figs. 12(a) and 12(b)]. Here it should be noted that the carrier mobility of Pt_2HgSe_3 is around 2000 cm^2/Vs, which is comparable to that of WTe_2 and two times larger than phosphorene and is therefore useful for device applications [43].

X. REALIZATION OF TOPOLOGICAL ZERO-LINE MODES

In principle, the so-called topologically protected interface states arise when an interface is designed between different topological phases such as between two QVH insulators with different valley-Chern numbers, between QSH and QVH insulators or even between two QSH insulators with different topologies. These topologically protected interface states are known as kink states or zero line modes. To discuss the possible realization of valley helical kink states, here we propose an interface between biased Pt_2HgSe_3 layers with opposite-field polarities on the left ($E_z < 0$) and right ($E_z > 0$) sides of the interface, see Fig. S7(a) in SM [35]. As shown by the schematic diagram in Fig. S7(a) in SM [35], in going from the left where QVH and QSH states exist simultaneously [$\Omega_z(K_+/K_-) \lessgtr 0$, $\mathcal{Z}_2 = 1$] to the right where also QVH and QSH states exist simultaneously but with opposite Berry curvatures at the two valleys [$\Omega_z(K_+/K_-) \gtrless 0$, $\mathcal{Z}_2 = 1$], a pure-valley zero line modes emerge at the interface. These zero line modes sustain dissipationless pure valley currents, which remains robust against the valley-conservation scattering.

Similarly, to realize the spin-valley helical kink states, next, we design an interface between the QVH insulator induced by the staggered type potential (not by the vertical electric field) and intrinsic QSH insulator. For applying staggering potential, we can grow Al_2S_3 on the left part of the Pt_2HgSe_3 layer, which converts the Pt_2HgSe_3 layer to a QVH insulating state with [$\Omega_z(K_+/K_-) \gtrless 0$, $\mathcal{Z}_2 = 0$], see Fig. S7(b) in SM [35]. On the other hand, the right part of the Pt_2HgSe_3 layer should be remained free-standing with no electric field to keep preserve its QSH features [$\Omega_z(K_+/K_-) = 0$, $\mathcal{Z}_2 = 1$]. Thus across the interface, spin-polarized valley helical kink states could be established. These states sustain a spin–valley-dependent current at the interface, which shows immunity against spin-independent scattering and long-range intravalley scattering. Very recently, the spin-valley helical kink states has been reported in bismuthene by alloy engineering [44].

XI. CONCLUSIONS

In conclusion, by breaking the inversion symmetry in the jacutingaite family (Pt_2HgSe_3 and Pd_2HgSe_3) using the following three different strategies: exposing to a vertical electric field, interfacing different layers in this family using the heterobilayer approach, and finally growing on a ferroelectric substrate with switchable electric polarization, we observed different versatile phenomena based on spin-valley locking, including the coexistence of quantum spin Hall and quantum valley Hall effects, valley spin-valve effect, layer crossover combined with spin crossover by an electric field and spin polarized constant energy contours with trigonal type distortion near the Fermi level. More importantly, the spin splittings, Berry curvatures, and spin textures are indeed reversible by switching the electric field orientation from $E_z > 0$ to $E_z < 0$. The effect of polarization reversal from $+P$ to $-P$, which significantly affects the electronic structure around the Fermi level such as the rigid shift of the band structure with hole doping (Ohmic-type behavior), is also discussed in the
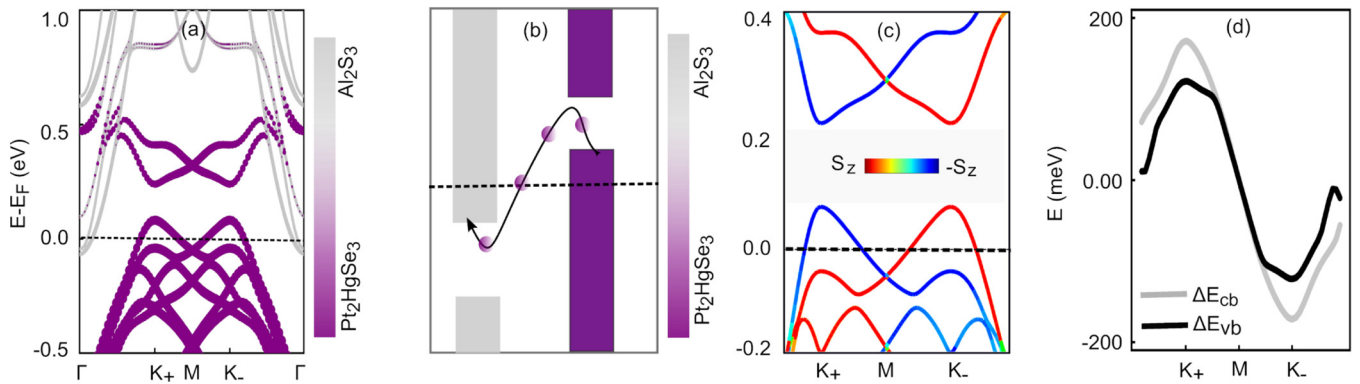
FIG. 12. (a) The layer resolved band structure of the Pt_2HgSe_3/Al_2S_3 heterobilayer in the presence of spin-orbit coupling effects in the $-P$ polarization state. The horizontal-dashed line represent the Fermi level. (b) The schematic representation of the Ohomic contact between the Pt_2HgSe_3 and Al_2S_3 layers. (c) Spin-resolved band structure of the Pt_2HgSe_3/Al_2S_3 heterobilayer for S_z spin component in the $-P$ polarization state. (d) The size of the momentum-dependent spin splitting in the top valence and lower conduction bands of the Pt_2HgSe_3 layer grown over the ferroelectric Al_2S_3 layer in the $-P$ polarization state.

jacutingaite family. The findings presented here may contribute to advance the spin-valley-based phenomena as highly demandable for spintronics and valleytronics applications.

[1] K. S. Novoselov, A. K. Geim, S. V. Morozov, D. Jiang, Y. Zhang, S. V. Dubonos, I. V. Grigorieva, and A. A. Firsov, Science **306**, 666 (2004).

[2] A. Molle, J. Goldberger, M. Houssa, Y. Xu, S.-C. Zhang, and D. Akinwande, Nat. Mater. **16**, 163 (2017).

[3] F. Pielnhofer, T. V. Menshchikova, I. P. Rusinov, A. Zeugner, I. Y. Sklyadneva, R. Heid, K.-P. Bohnen, P. Golub, A. I. Baranov, E. V. Chulkov *et al.*, J. Mater. Chem. C **5**, 4752 (2017).

[4] A. Zhao and B. Wang, APL Mater. **8**, 030701 (2020).

[5] P. Högl, T. Frank, K. Zollner, D. Kochan, M. Gmitra, and J. Fabian, Phys. Rev. Lett. **124**, 136403 (2020).

[6] X. Zhai and Y. M. Blanter, Phys. Rev. B **101**, 155425 (2020).

[7] M. U. Rehman and Z. Qiao, Eur. Phys. J. B **91**, 42 (2018).

[8] Majeed Ur Rehman and A. A. Abid, Chin. Phys. B **26**, 127304 (2017).

[9] M. Z. Hasan and C. L. Kane, Rev. Mod. Phys. **82**, 3045 (2010).

[10] X. Xu, W. Yao, D. Xiao, and T. F. Heinz, Nat. Phys. **10**, 343 (2014).

[11] C. M. Gilardoni, F. Hendriks, C. H. van der Wal, and M. H. D. Guimaraes, Phys. Rev. B **103**, 115410 (2021).

[12] I. Žutić, J. Fabian, and S. Das Sarma, Rev. Mod. Phys. **76**, 323 (2004).

[13] D. Xiao, G. B. Liu, W. Feng, X. Xu, and W. Yao, Phys. Rev. Lett. **108**, 196802 (2012).

[14] A. Marrazzo, M. Gibertini, D. Campi, N. Mounet, and N. Marzari, Phys. Rev. Lett. **120**, 117701 (2018).

[15] I. Cucchi, A. Marrazzo, E. Cappelli, S. Ricco, F.Y. Bruno, S. Lisi, M. Hoesch, T.K. Kim, C. Cacho, C. Besnard, E. Giannini, N. Marzari, M. Gibertini, F. Baumberger, and A. Tamai, Phys. Rev. Lett. **124**, 106402 (2020).

[16] F. Crasto de Lima, R. H. Miwa, and A. Fazzio, Phys. Rev. B **102**, 235153 (2020).

[17] K. Kandrai, P. Vancso, G. Kukucska, J. Koltai, G. Baranka, A. Hoffmann, A. Pekker, K. Kamaras, Z. E. Horvath, A. Vymazalova *et al.*, Nano Lett. **20**, 5207 (2020).

[18] A. Vymazalova, F. Laufek, M. Drabe, A. R. Cabral, J. Haloda, T. Sidorinova, B. Lehman, H. F. Galbiat, and J. Drahokoupil, Can. Mineral. **50**, 431 (2012).

[19] J. I. Facio, S. K. Das, Y. Zhang, K. Koepernik, J. van den Brink, and I. C. Fulga, Phys. Rev. Materials **3**, 074202 (2019).

[20] A. Marrazzo, N. Marzari, and M. Gibertini, Phys. Rev. Research **2**, 012063(R) (2020).

[21] Z. Liu, Y. Han, Y. Ren, Q. Niu, and Z. Qiao, Phys. Rev. B **104**, L121403 (2021).

[22] M. U. Rehman, Z. Qiao, and J. Wang, Phys. Rev. B **105**, 165417 (2022).

[23] J. Jung, F. Zhang, Z. Qiao, and A. H. MacDonald, Phys. Rev. B **84**, 075418 (2011).

[24] Y. Ren, Z. Qiao, and Q. Niu, Rep. Prog. Phys. **79**, 066501 (2016).

[25] L. L. Tao and E. Y. Tsymbal, Phys. Rev. B **100**, 161110(R) (2019).

[26] T. Cao, G. Wang, W. Han, H. Ye, C. Zhu, J. Shi, Q. Niu, P. Tan, E. Wang, B. Liu, and J. Feng, Nat. Commun. **3**, 887 (2012).

[27] Z. R. Gong, G. B. Liu, H. Y. Yu, D. Xiao, X. D. Cui, X. D. Xu, and W. Yao, Nat. Commun. **4**, 2053 (2013).

[28] M. Gmitra, D. Kochan, P. Hogl, and J. Fabian, Phys. Rev. B **93**, 155104 (2016).

[29] M. Gmitra and J. Fabian, Phys. Rev. Lett. **119**, 146401 (2017).

[30] P. E. Blöchl, Phys. Rev. B **50**, 17953 (1994).

[31] G. Kresse and J. Furthmuller, Phys. Rev. B **54**, 11169 (1996).

[32] A. A. Mostofi, J. R. Yates, Y. S. Lee, I. Souza, D. Vanderbilt, and N. Marzari, Comput. Phys. Commun. **178**, 685 (2008).

[33] G. Pizzi, V. Vitale, R. Arita, S. Blugel, F. Freimuth, G. Geranton, M. Gibertini, D. Gresch, C. Johnson, T. Koretsune *et al.*, J. Phys.: Condens. Matter **32**, 165902 (2020).

[34] Q. Wu, S. Zhang, H.-F. Song. M. Troyer, A. A. Soluyanov, Comput. Phys. Commun. **224**, 405 (2018).

[35] See Supplemental Material at http://link.aps.org/supplemental/10.1103/PhysRevB.105.195439 for detailed computational methods, electrically switchable spin splittings and spin texture maps of Pd$_2$HgSe$_3$ layer, geometrical structures of the Pt$_2$HgSe$_3$/Pd$_2$HgSe$_3$ and Pt$_2$HgSe$_3$/Al$_2$S$_3$ heterobilayers, and possible realization of valley Hall kink states and spin valley Hall kink states in the jacutingaite family, which includes Refs. [45–49].

[36] X. Li, T. Cao, Q. Niu, and J. Feng, Proc. Natl. Acad. Sci. USA **110**, 3738 (2013).

[37] Y. Feng, Q. Jiang, B. Feng, M. Yang, T. Xu, W. Liu, X. Yang, M. Arita, E. F. Schwier, K. Shimada *et al.*, Nat. Commun. **10**, 4765 (2019).

[38] W. Ding, J. Zhu, Z. Wang, Y. Gao, D. Xiao, Y. Gu, Z. Zhang, and W. Zhu, Nat. Commun. **8**, 14956 (2017).

[39] F. Xue, W. Hu, K. C. Lee, L.-S. Lu, J. Zhang, H.-L. Tang, A. Han, W.-T. Hsu, S. Tu, W.-H. Chang *et al.*, Adv. Funct. Mater. **28**, 1803738 (2018).

[40] T. Frank, P. Hogl, M. Gmitra, D. Kochan, and J. Fabian, Phys. Rev. Lett. **120**, 156402 (2018).

[41] T. Arakane, T. Sato, and S. Souma, Nat. Commun. **3**, 636 (2012).

[42] X. Wu, M. Fink, W. Hanke, R. Thomale, and D. Di Sante, Phys. Rev. B **100**, 041117(R) (2019).

[43] D. Mauro, H. Henck, M. Gibertini, M. Filippone, E. Giannini, I. G. Lezama, and A. F. Morpurgo, 2D Mater. **7**, 025042 (2020).

[44] T. Zhou, S. Cheng, M. Schleenvoigt, P. Schuffelgen, H. Jiang, Z. Yang, and I. Zutic, Phys. Rev. Lett. **127**, 116402 (2021).

[45] J. P. Perdew, J. A. Chevary, S. H. Vosko, K. A. Jackson, M. R. Pederson, D. J. Singh, and C. Fiolhais, Phys. Rev. B **46**, 6671 (1992).

[46] S. Grimme, J. Antony, S. Ehrlich, and S. Krieg, J. Chem. Phys. **132**, 154104 (2010).

[47] U. Herath, P. Tavadze, X. He, E. Bousquet, S. Singh, F. Munoz, and A. H. Romero, Comput. Phys. Commun. **251**, 107080 (2020).

[48] H.-J. Kim, VASPBERRY Code, Version V1.0 (2018), https://github.com/Infant83/VASPBERRY.

[49] R. Longuinhos, A. Vymazalova, A. R. Cabral, and J. Ribeiro-Soares, J. Phys.: Condens. Matter **33**, 065401 (2021).